Powder-Shape Analysis and Sintering Behavior of High-Density Polyethylene Powders for Rotational Molding

Antonio Greco, Alfonso Maffezzoli

Dipartimento di Ingegneria dell'Innovazione, Università degli Studi di Lecce, Via per Arnesano, Lecce, Italy

Received 3 July 2003; accepted 25 August 2003

ABSTRACT: The quality of rotational molded products is strongly affected by the sintering behavior of the powders used in the process. In turn, for a given material, the sintering behavior of polymer powders is dependent on the size and the shape of particles obtained in the milling apparatus. The quality of powders for rotational molding is usually determined by means of size distribution, dry flow, and bulk density tests. However, these tests do not provide insight into the relationship between the shape of powders, the milling conditions, and the sintering behavior during the rotational molding cycle. Nevertheless, the application of mathematical tools to powder analysis can significantly improve the efficiency of the grinding process, looking not only at the size but also at the shape of the powder. This can in turn result in a higher reliability of rotational molding and in better performances of the products obtained in processes dominated by the sintering behavior of polymer powders. In this work the grinding process of recycled high-density polyethylene was analyzed using a quantitative approach to the shape and size of the powders. In particular, shape factors, capable of characterizing powders obtained in different milling conditions, were studied. Finally, the influence of the powders' shape and size on sintering behavior was studied by thermomechanical analysis. © 2004 Wiley Periodicals, Inc. J Appl Polym Sci 92: 449–460, 2004

Key words: polyethylene (PE); rotational molding; powders; kinetics (polym.); thermomechanical analysis (TMA)

INTRODUCTION

Rotational molding is a unique technology for the production of hollow or double-wall parts, usually of large dimensions.[1] The process involves the rotation of a mold, filled with a polymer powder in a heating oven, where the polymer reaches its melting temperature. A sintering-like process in the melt state promotes densification of polymer powders[2] through a double-stage mechanism involving powder coalescence[3–5] and bubble removal.[6] Once a fully dense polymer layer is obtained, the mold is cooled to room temperature before the extraction of the part. Heat-transfer phenomena through the powder mass, sintering efficiency, and surface quality of the products are strongly affected by the nature of the polymer, and by the size and the shape of the powders used.[7,8]

The time needed for the heat to penetrate within the center of a polymer particle is mainly determined by its size. As a consequence, larger particles will need a longer time to reach the temperature necessary to promote melting and subsequent coalescence.[7] Further, a complete sintering of powders (i.e., void fraction equal to zero) is very difficult to obtain for large particles.[3] In fact, an efficient bubble-removal process is more critical for larger particles[6,7] because of the higher initial dimension of voids. On the other hand, very small particles are very difficult to obtain, as a consequence of very long grinding times and energy consumption.[8] Usually powders with a well-determined size distribution are needed to achieve a good packing of the polymer mass and efficient sintering.[7]

The shape of the particles also plays a significant role during the heating cycle of the rotational molding process. Two counteracting factors influence the thermal conductivity of powders. Because the contact area between particles increases with the shape irregularity, irregularly shaped powders are characterized by an improved heat transfer between particles.[8,9] On the other hand, irregular shapes can result in a less-efficient packing of the material,[10] promoting an increased porosity, a lower apparent density, and finally a decrease of the thermal conductivity of powders.[9,11–13] This effect very often counterbalances the potential increase of thermal conductivity related with a higher contact area. The actual thermal conductivity of the powder will depend on the relative intensity of both effects, the thermal conductivity in the solid polymer phase, and the amount of entrapped gas.[9]

The relevance of the powders' shape and size makes the grinding process particularly critical for the deter-

Correspondence to: A. Maffezzoli (alfonso.maffezzoli@unile.it).

Journal of Applied Polymer Science, Vol. 92, 449–460 (2004)

mination of the quality of the parts and cycle times during rotational molding.[7] The grinding temperature is the factor that mainly affects the powders' size and shape.[7,14] Other parameters, such as mill speed, gap size, and number of teeth on the grinding plates, have a weak influence on the final powder quality.[14] Temperature fluctuations during milling are mainly caused by the frictional heating between the cutting plates and the polymer pellets, and by the viscous dissipation associated with particle shearing and drawing. The quality of the powders for rotational molding is usually determined by means of particle size distribution, bulk density, dry flow,[7] and internal friction angle.[15] Only a few attempts have been made to use microscopy to characterize the shape and the size of powders.[15] On the other hand, a number of different techniques, such as fractal analysis,[16–19] moment invariants,[20–24] Fourier descriptors,[25–27] and wavelet analysis,[28,29] have been developed to describe irregular morphologies through image analysis.

In this work the grinding process of recycled high-density polyethylene (rHDPE) was studied by means of optical microscopy. Powders were characterized through their bidimensional projection on the plane perpendicular to the direction of the light of the microscope. Different shape factors, capable of characterizing powders obtained at different temperatures, were studied. Finally, the influence of the powders' shape and size on sintering behavior was studied by thermomechanical analysis (TMA).

EXPERIMENTAL

The material used was recycled HDPE, blow-molding grade, which was shown to be a cost-effective raw material for rotational molding, blended with a linear low-density polyethylene.[30] The material was ground by means of an ultracentrifugal mill ZM100 by Retsch. The temperature inside the mill, mainly determined by the feed rate of rHDPE pellets, was controlled by placing a thermocouple on the sieve. In the present study, three milling temperature ranges were selected: $T < 40$°C; 60°C $< T <$ 70°C; 90°C $< T <$ 110°C. Powders obtained at these temperatures were labeled as type "L," "M," and "H," respectively. The mesh size of the sieve of the grinder was 0.5 mm. A further sieving on type H powders was also performed after grinding because powder coalescence phenomena on the external side of the sieve during milling caused the presence of a high fraction of particles having $d > 0.5$ mm. About 50% of the powders of type H were discarded.

In this study the particle analysis was applied at the two-dimensional (2D) level operating on 2D microscope images. A statistically significant number of photographs (40 for each sample) was taken for powders obtained at different temperatures using an optical microscope (Epiphot 200). Photographs were then elaborated through the image analysis software Paint Shop Pro. Histogram adjustment was applied for the conversion of the gray-scale image into a black and white binary image. The image was then converted to a 256 × 187 matrix, and particle analysis was performed on the area and the perimeter of each particle. For characterization of powders Heywood criteria, fractal analysis, and wavelet descriptors were used, applying user-defined Matlab functions to the area and the perimeter of each particle.

The efficiency of the sintering process for L, M, and H powders was studied through a Perkin–Elmer TMA 8 thermomechanical analyzer (TMA; Perkin Elmer Cetus Instruments, Norwalk, CT). Samples of about 10 mg corresponding to an initial thickness of about 1 mm, were used. Heating scans were run between 40 and 200°C at 3, 5, and 10°C/min. To better simulate the zero-pressure sintering condition occurring during rotational molding the lowest possible pressure on the sample was used (35 Pa). Powder sintering under the TMA probe was performed using small aluminum pans (standard DSC sample pans) limiting the powder shrinkage in one direction. Therefore the density $\rho(t)$ was calculated as a function of initial density ρ_i from the ratio between the thickness of the sample at the beginning of the test L_i and the thickness at time t, $L(t)$ as expressed in eq. (1):

$$\rho(t) = \rho_i \frac{L_i}{L(t)} \tag{1}$$

Each result reported was calculated as the average of three tests.

Differential scanning calorimetry (DSC) was used to study the melting behavior of rHDPE. Samples about 10 mg were heated in an inert atmosphere from 20 to 250°C at a scanning rate of 10°C/min. The onset and the peak temperatures of melting were evaluated, to highlight the inherent differences between the two distinct processes.[31]

Mathematical tools for powder analysis

Heywood criteria

Once the perimeter and the area of powder images were extracted, the shape factors, called Heywood criteria,[15] were used to characterize the particle shape. Three parameters were adopted: circularity, roundness, and aspect ratio (or elongation), defined in eqs. (2)–(4):

$$\text{Circularity} = \frac{4\pi \text{ Area}}{\text{Perimeter}} \tag{2}$$

$$\text{Roundness} = \frac{\text{Area}}{\pi \frac{(D_{\max})^2}{4}} \quad (3)$$

$$\text{Elongation} = \frac{D_{\max}}{D_{\min}} \quad (4)$$

where $D_{\max}$ and $D_{\min}$ are the maximum and minimum Feret diameter of the particle, as defined by Janowsky et al.[32] Given a 2D area, at each direction $\vec{n}$ can be associated with a Feret diameter, defined as the minimum distance between two parallel lines perpendicular to the $\vec{n}$ direction, which enclose the area. To find the Feret diameter for each direction the image was rotated between 0 and 180° with a 1° step. Each rotation angle i corresponds to a rotation of the $\vec{n}$ direction of 1°. The Feret diameter at each rotation angle i was evaluated according to eq. (5):

$$D_{f,i} = \max[d(y_A, y_B)] \quad A, B \in P_i \quad (5)$$

where $d(y_A, y_B)$ is the distance between points and P_i is the perimeter of the particle at a given rotation angle i. The maximum Feret diameter was determined as the maximum value of $D_{f,i}$ over different rotation angles, as reported in eq. (6):

$$D_{\max} = \max_{0 \le i \le 180} (D_{f,i}) \quad (6)$$

whereas the minimum Feret diameter was taken as the diameter in the direction perpendicular to that one corresponding to $D_{\max}$.

The aim of Heywood parameters is to emphasize the spherical (circularity and roundness) or the oblate (elongation) shape of a particle. Circularity, roundness, and elongation are equal to unity for a spherical shape. Both circularity and roundness decrease while the particle deforms from an ideal spherical shape, whereas elongation increases. The limit of these parameters is that they give a rough indication of the shape of a particle as a whole, although they do not provide indication of the regularity of a particle at a finer observation scale.

Fractal analysis

In this work the Mandelbrot method[16] was used, based on a Richardson plot, where the estimated length of a contour is plotted as a function of the scale of the measurement on a double-log scale. If a profile is approximated piecewise linearly, its perimeter increases with decreasing step length, that is, with the length of the side of the equilateral polygon that approximates the profile. A simple relation can be established between the estimated length $L(\varepsilon)$ and the step length ε, expressed as

$$L(\varepsilon) = M\varepsilon^{(1-D)} \quad (7)$$

where M is a positive constant and D is a constant ≥ 1. By linear regression of experimental data on a double-logarithm plot of $L(\varepsilon)$ versus ε, the value of D, called the fractal dimension, can be determined. The procedure used in this work to determine at each step length the estimated contour length is the same as that described by Allen et al.[16] The minimum step length was chosen to be 2 pixels, corresponding to 5.9 μm, the maximum equal to a half of the maximum Feret diameter. Further, at each step length, the perimeter was calculated starting from every point of the contour, and the average value was taken as the estimated length,[33] according to eq. (8):

$$L(\varepsilon) = \operatorname*{avg}_{1 \le n \le N-1} [L(\varepsilon, n)] \quad (8)$$

where n is the position of the starting point on the contour and N is the total number of points in the contour. In this way, the calculated estimated perimeter was made invariant from the choice of the starting point.[33] Richardson plots for powders L, M, and H are shown in Figure 1. If a particle is self-similar (i.e., its degree of roughness is the same for all scales of observation), one line can be drawn through all data points. Particle contours, however, rarely provide self-similarity[19]; more commonly the fractal dimension is dependent on the step length interval over which it is evaluated and the slope of the Richardson plot changes with the step length. As a consequence of this, a textural dimension D_{tex} was determined as the slope of the Richardson plot at the lower step length interval, corresponding to the finer observation scale, whereas at larger scales a structural dimension D_{struct} was determined.[17,33,34] In this work the textural dimension was evaluated as the slope of the Richardson plot at the seven lower step lengths, whereas the structural dimension was evaluated as the slope of the plot at the seven higher step lengths, as shown in Figure 1 for powders H. The Richardson plot for a circle is also shown in Figure 1. A linear fit of the Richardson plot for a circle simply provides $D = 1.00$ at each observation scale, which actually means absence of fractality.[17]

Fourier descriptors and wavelet analysis

When the contour of a particle is extracted from the image, a periodic function is obtained in the x–y coordinates. Each point of the contour has coordinates $[x(n), y(n)]$, where n is the position on the contour. In the complex plane the representation of each point is

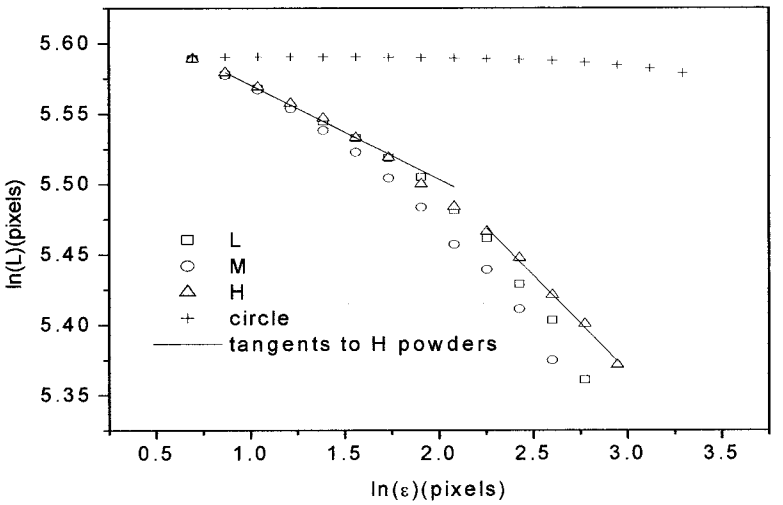

Figure 1 Richardson plot for powders L (□), M (○), and H (△), and for a circle (+) and linear fit of H powders plot (—).

given as $z(n) = x(n) + jy(n)$. The complex Fourier transform of $z(n)$ can be written as in eq. (9)[27]:

$$F(k) = \frac{1}{N}\sum_{n=0}^{N-1} z(n)\exp(-j2\pi kn/N) \quad 0 \le k \le N-1 \tag{9}$$

where k is the order of the descriptor and N is the total number of points. The coefficients $F(k)$ need to be independent from the choice of the starting point, and from rotation, translation, and scaling of the contour. The calculation of real first-order Fourier descriptors of the coordinate points $x(n)$ and $y(n)$[25] leads to the determination of the centroid position of the contour, and the phase angles necessary to make the profile invariant from rotation and starting point. The scale-invariant feature was determined as the average of the two major axes of the first-order ellipsoid. Once these parameters were determined, Fourier descriptors were made invariant following the procedure described by Lai et al.[26] Once Fourier descriptors of particle shape have been determined, wavelet analysis allows the determination of contour irregularities corresponding to different scales as a function of the position on the contour. The wavelet analysis is based on the calculation of the correlation between the signal $z(n)$ and a test function, $\omega(n)$, called the wavelet function. The correlation coefficient is defined in eq. (10):

$$a(n) = \int_{-\infty}^{\infty} z(\tau)\omega(\tau - n)\, d\tau \tag{10}$$

The coefficient $a(n)$ provides information about the structure of $z(n)$ and its relationship with the test wavelet $\omega(n)$. When z correlates with ω then $a(n)$ is large; otherwise $a(n)$ is small.[29] Among all wavelet functions, the harmonic wavelet was used in this work for its simplicity. A harmonic wavelet is such that its Fourier transform is zero everywhere, except in a finite band of frequency, defined by $2\pi m \le k < 2\pi l$, with $m \le l$ need not be integers. In this range, the Fourier transform of the wavelet function has a constant value $W(k) = 1/[2\pi(l - m)]$. If the total number of points on the contour is a power of 2, $N = 2^J$, where J is a positive integer, the correlation coefficients can be written as[28,35]

$$\begin{aligned} a_0 &= F(0) \\ a_{2^j+n} &= \sum_{s=0}^{2^j-1} F(2^j + s)\exp(i2\pi sn/2^j) \\ \bar{a}_{2^j+n} &= \sum_{s=0}^{2^j-1} F(N - 2^j - s)\exp(-i2\pi sn/2^j) \\ a_{N/2} &= F(N/2 + 1) \end{aligned} \tag{11}$$

where $0 \le j \le J - 2$ is the resolution level and $0 \le n \le 2^j - 1$ is the position on the contour. Consequently, each profile can be approximated by $(J - 1)$ different resolution levels. The total roughness associated with each resolution level j can be calculated as the energy of the level[28] and is reported in eq. (12):

$$R_j = \frac{1}{2^j}\sum_{n=0}^{2^j-1} (|a_{2^j+n}|^2 + |\bar{a}_{2^j+n}|^2) \tag{12}$$

with $0 \le j \le J - 2$. The energy associated with resolution level 0 is an indication of the elongation of a particle (ranging from 1 for a circle to 2 for a slab), increasing elongation resulting in higher energies. At

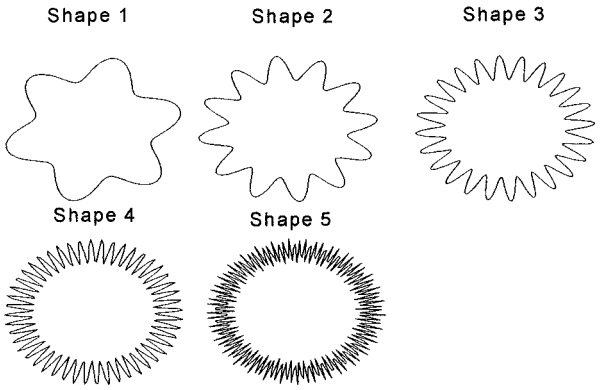

Figure 2 Shapes obtained adding a secondary wave to a circle, used for Wavelet analysis verification.

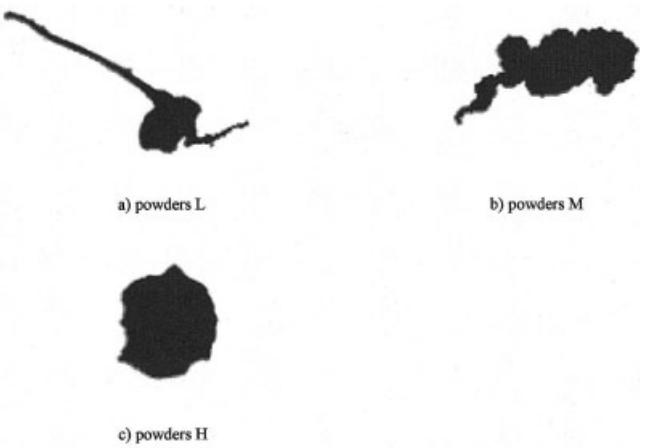

Figure 3 Particle shapes from optical microscopes for powders L, M, and H.

higher resolution levels, which correspond to observations at finer scales, increasing energy corresponds to higher roughness at that level.

The efficiency of wavelet analysis in particle analysis was tested on five different shapes, obtained adding secondary waves of different frequencies to a circle. The different shapes are shown in Figure 2 as Shape 1–Shape 5. The energies at seven different resolution levels for the shapes of Figure 2 are reported in Table I. From the results reported in Table I it can be observed that wavelet analysis leads to the determination of a distribution of energies as a function of the resolution level. The position of the energy peak depends on the frequency window corresponding to the higher roughness, and its amplitude depends on the intensity of the roughness. The energy associated with level 0 is always 1, given that all the shapes are derived from a circle and their elongation is 1. On the other hand, increasing the frequency of the secondary wave in Figure 2 results in a shift of the maximum energy to higher-resolution levels. The peaks for the five shapes reported in Figure 2 differ only for their localization on the frequency scale, and not for their absolute amplitude because the amplitude of the secondary wave is the same for all the shapes of Figure 2.

For analysis of HDPE powders the contour of each particle image was sampled to obtain for each profile a total number of points $N = 256$. In this way, for each image, seven shape features were obtained. Because at the higher-resolution levels the value of the energy can be strongly affected by the pixel resolution of the image, only five features were extracted, corresponding to the lower five resolution levels.

RESULTS AND DISCUSSION

Characterization of powders

Typical particle shapes for the powders obtained at different temperatures are shown in Figure 3. When polyethylene is ground, the particles are sheared between cutting elements, and long tails are drawn as a consequence of the toughness of the material. At lower temperatures, the viscosity of the material is too high to allow any rearrangement of the shape, capable of lowering the surface energy toward a spherical shape, as is evident from Figure 3(a). As a consequence, particles obtained at room temperature have a rough surface and irregular shape. At higher temperatures

TABLE I
Wavelet Energy as a Function of Resolution Level for the Different Shapes of Figure 2

Resolution level	Wavelet energy				
	Shape 1	Shape 2	Shape 3	Shape 4	Shape 5
0	1	1	1	1	1
1	2.29E-5	2.21E-5	2.20E-5	2.20E-5	2.20E-5
2	0.0199	7.38E-6	5.61E-6	5.37E-6	5.32E-6
3	1.86E-5	0.0199	6.60E-6	2.71E-6	2.22E-6
4	2.88E-6	1.88E-5	0.0199	9.02E-6	1.39E-6
5	1.37E-6	4.27E-6	3.17E-5	0.0198	6.78E-6
6	9.31E-7	2.64E-6	1.03E-5	7.03E-5	0.0199

TABLE II
Numerical Values of Heywood Criteria, Fractal Dimensions, and Wavelet Energies for Powders L, M, and H

	Powders L	Powders M	Powders H
	Heywood criteria		
Area $\times 10^{-2}$ (mm^2)	4.95 ± 2.19	4.32 ± 2.04	9.75 ± 2.90
Circularity	0.267 ± 0.148	0.415 ± 0.162	0.472 ± 0.0921
Roundness	0.297 ± 0.172	0.462 ± 0.143	0.541 ± 0.0898
Elongation	2.29 ± 1.07	1.63 ± 0.390	1.51 ± 0.219
	Fractal analysis		
D	1.17 ± 0.0426	1.15 ± 0.0492	1.12 ± 0.0319
D_{tex}	1.07 ± 0.0232	1.08 ± 0.0251	1.07 ± 0.0162
D_{struct}	1.38 ± 0.149	1.25 ± 0.110	1.20 ± 0.0727
	Wavelet analysis		
R_0	1.16 ± 0.179	1.06 ± 0.0981	1.02 ± 0.0237
R_1	0.113 ± 0.118	0.0639 ± 0.0623	0.0284 ± 0.0172
R_2	0.0199 ± 0.0216	0.0166 ± 0.0187	0.0103 ± 0.00635
R_3	0.00270 ± 0.00250	0.00277 ± 0.00219	0.00218 ± 0.00106
R_4	4.22E-4 ± 2.98E-4	4.42E-4 ± 3.83E-4	3.52E-4 ± 1.65E-4

the tails, which are formed during milling, can shrink and recoil into the main particle body[14]: the oriented and anisotropic polymer chains of the tails assume a nonoriented and isotropic configuration. This allows cleaner cuts and smoother surfaces on particles characterized by lower elongation, as can be seen in Figure 3(b). Further increasing of the temperature can lead to premature melting and adhesion of the powders,[36] and consequently to the formation of clusters, which are not suitable for rotational molding.[7] This leads to particles having higher dimension, but more regular shapes, as can be seen in Figure 3(c).

The occurrence of the typical shapes reported in Figure 3 is confirmed from the results of Table II, where the Heywood criteria, fractal dimensions, and wavelet energies at different resolution levels are shown for L, M, and H powders.

A minimum value for the area of the particles was obtained for powders M ground at a temperature of about 65°C. For particles H the average size was higher compared with that of powders M and L. This can be attributed to some coalescence of particles, as a consequence of the high temperature.

The elongation decreased going from samples L to samples H. The "compactness" factors, roundness and circularity, increased with increasing temperature. This was confirmed from the observation of wavelet energy at resolution levels 0 and 1, which were directly related to the elongation of a particle and to the presence of tails, both parameters increasing with de-

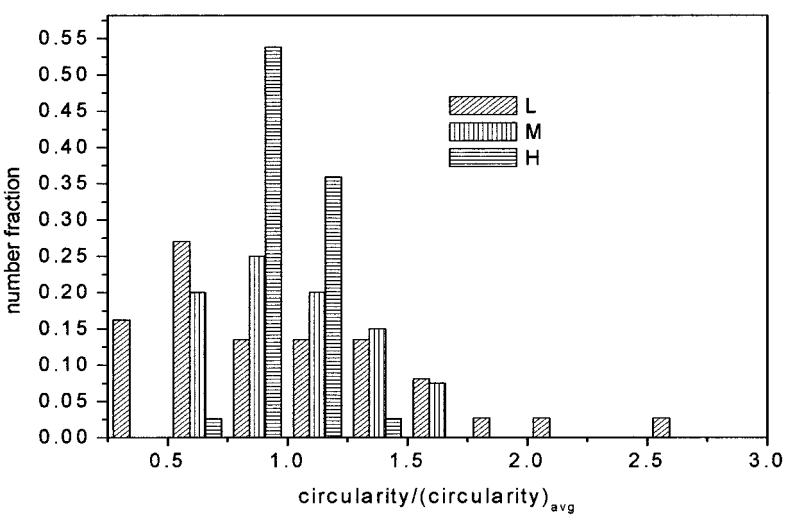

Figure 4 Normalized distribution of circularity for powders L (▨), M (▥), and H (▤).

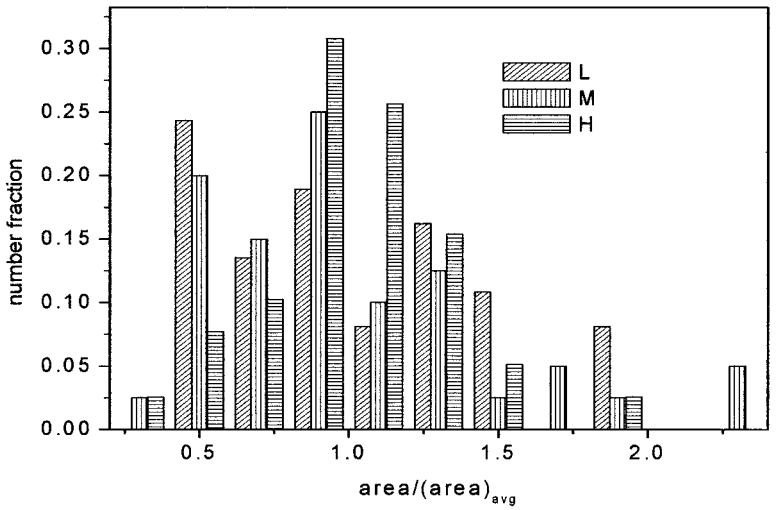

Figure 5 Normalized distribution of area for powders L (▨), M (▥), and H (▤).

creasing milling temperature. This indicates that more regular particles can be obtained at higher temperatures, whereas at lower temperatures the particles are highly elongated.

The structural dimension decreased going from powders L to powders H, indicating that the roughness of the samples decreased with increasing temperature. This was confirmed by the wavelet energies at higher-resolution levels, R_1 and R_2, also decreasing with increasing temperature. The roughness at a finer scale, which is related to the textural dimension D_{tex} reported in Table II, and to the energies at higher-resolution levels (R_3 and R_4), was almost the same for powders L, M, and H, indicating that the difference is not as evident as for the roughness at lower resolution. At resolution levels corresponding to textural dimension and to the energies at levels 3 and 4, errors can be generated by the resolution of the image, by the contour acquisition technique,[33] and by the noise related to the low magnification of the image.[28] As a consequence, the importance of these parameters must not be emphasized.

From the standard deviation values of Heywood criteria, also reported in Table II, it can be observed that more uniformly distributed shapes can be obtained at higher temperatures, whereas for powders L and M both regularly and irregularly shapes are present. Further, the same behavior is observed in Table II for structural dimension and wavelet energy up to level 3. This is better evidenced in Figure 4, where the distribution for the circularity is shown. At higher grinding temperatures, irregularly shaped particles can reach low surface energy conformations because of the higher mobility of polymer chains at-

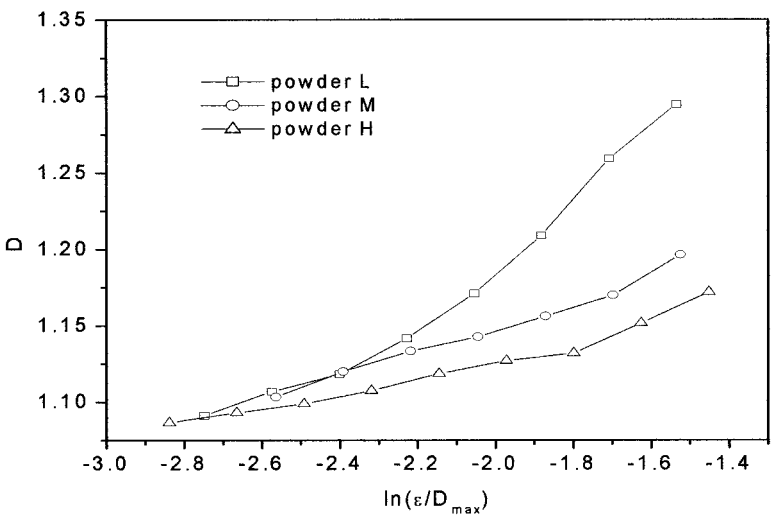

Figure 6 Fractal dimension as a function of step length interval for powders L (—□—), M (—○—), H (—△—).

TABLE III
Mean Values of Elongation and R_1 for Powders L at Different Populations of Analyzed Particles

Number of particles	Elongation	R_1
5	2.351	0.1747
10	2.034	0.1156
15	2.029	0.1019
20	2.108	0.09432
25	2.162	0.1203
30	2.248	0.1155
35	2.304	0.1141
40	2.290	0.1128

tained also after particle production. At lower temperature, this rearrangement is not possible, and both regularly and irregularly shaped particles are present. A different behavior is found for the area distributions, shown in Figure 5. Broad distributions are obtained for any powder sample, as a consequence of nonuniform milling process and temperature.

To better investigate the fractal nature of particles, the approach described by Kindratenko et al.[17] was applied to study the variation of fractal dimension with step length range. Results are reported in Figure 6, where the average value of the fractal dimension is reported as a function of the step length, normalized with respect to the maximum Feret diameter, for powders L, M, and H. The fractal dimension was calculated at each step length from a linear regression on the adjacent five points. As may be observed in Figure 6, the fractal dimension does not show a neat distinction between a textural and a structural dimension, but rather a continuous increase with increasing step length. As a consequence of this, the textural and structural dimensions reported in Table II can be regarded as extreme values of a distribution of fractal dimensions. Also in this case, as already underlined for the wavelet descriptors, the observation scale plays a significant role, given that at different resolution levels different slopes of the Richardson plot can be found.[19]

At low step length the three samples L, M, and H show no difference, as confirmed from the observations on the textural dimension and wavelet energies at high resolution, reported in Table II. With increasing step length the higher slopes, which can be observed with decreasing milling temperature, are responsible for the higher structural dimension for powders L, as confirmed by Heywood criteria and wavelet energies at lower resolutions.

The influence of the number of analyzed particles on the calculated shape factors was also assessed, analyzing the evolution of the average value for elongation and R_1 with increasing population of tested particles. The results are reported in Table III for powders L. Particles L were chosen for this purpose for their higher heterogeneity with respect to powders M and H. In Table III it can be observed that the difference between consecutive populations decreases with increasing number of analyzed particles. Analyzing 35 or 40 particles results in a difference in the average of 0.6 and 1.2% for elongation and R_1, respectively. Further, for any sample the mean is within experimental mean deviation, reported in Table II for the sample containing 40 particles. As a consequence of these observations, the selected population of 40 samples for each milling temperature was considered to be representative of the whole population.

Characterization of powder sintering by TMA

TMA sintering experiments were performed on the HDPE powders of different shapes. The bulk density of powders was determined by dividing the weight of each sample for its volume at room temperature (reported in Table IV). The bulk density of powders increases with increasing grinding temperature. This result is consistent with the shape measurements: highly regular shaped powders are characterized by a more efficient packing, in which the fraction of voids is much lower than that for irregularly shaped particles,[10] characterized by tail bridging and higher interparticle friction[37] and surface roughness.

The derivative of the linear shrinkage dL/dT measured in a TMA experiment at 10°C/min is compared in Figure 7 with the DSC melting endotherm performed at the same heating rate. Sintering is observed only when the sample temperature exceeds the onset of melting temperature, as previously observed for other semicrystalline polymers.[5] Sintering can occur only if a finite viscosity is achieved, as predicted by the Frenkel model.[3] After melting has begun, the sintering rate dL/dt suddenly increases as a consequence of high initial void fraction and viscosity reduction, and reaches its maximum at a temperature lower than

TABLE IV
Initial and Final States for the Numerical Integration of Eqs. (13)–(15)

Parameter	Powders L	Powders M	Powders H
Initial bulk density (kg/m^3)	300.5 ± 4.94	325.5 ± 9.31	347.1 ± 5.56
Final void fraction	0.01233	0.00895	0.02375
Average bubble dimension (μm^2)	5715 ± 2712	6725 ± 3742	7754 ± 6452

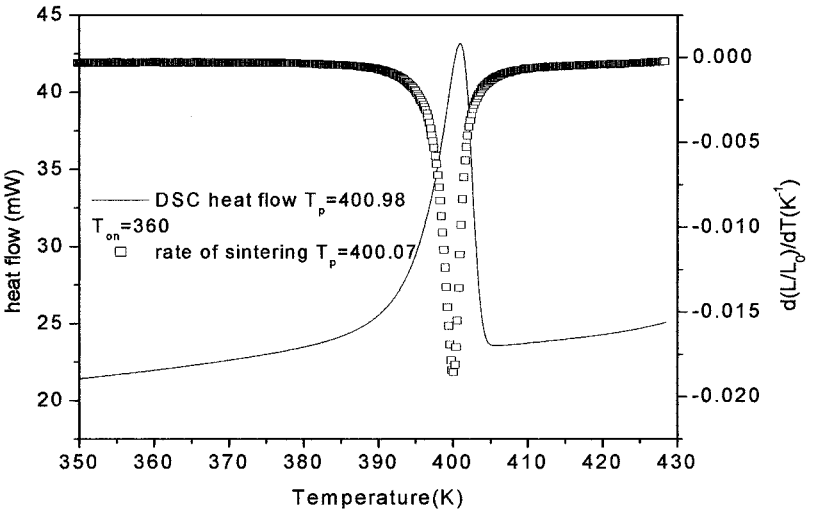

Figure 7 DSC melting endotherm (—) and TMA rate of sintering (□) for powders H.

the peak temperature determined from DSC, which is mainly determined by the lamellar thickness distribution of crystals.[30] In Figure 8 and Figure 9 the sintering behavior of powders in terms of linear contraction and rate of contraction is shown for powders obtained at different temperatures. The results reported in Figure 9 were obtained by differentiating the measured shrinkage of Figure 8.

Surface area reduction is the driving force for sintering, and thus finer particles with high surface area are expected to sinter more rapidly.[38] Moreover, higher dimensions cause higher-temperature gradients within a single particle,[39] leading to increased sintering temperatures.[40,41] This is confirmed from the results of Figure 9, where it can be observed that for powders H the peak temperature is about 2.3°C higher than the peak temperature for powders L. This phenomenon was observed at every heating rate. Further, once coalescence of powders has been completed, the initial larger dimension of bubbles entrapped in the molten mass is responsible for longer densification times[6] or not fully sintered samples,[3] as shown in Figure 8, where less-efficient sintering is observed with increasing size of powders.

Optical micrographs of sintered samples were taken, and the void fraction and area distribution of air bubbles on the surface were evaluated. Images of the sintered samples for powders L, M, and H, are shown in Figure 10. The results obtained for the final void fraction and bubble dimension were calculated as an average over four surfaces (reported in Table IV).

The void fraction for the sintered samples of H powders is higher than that of the other powders.

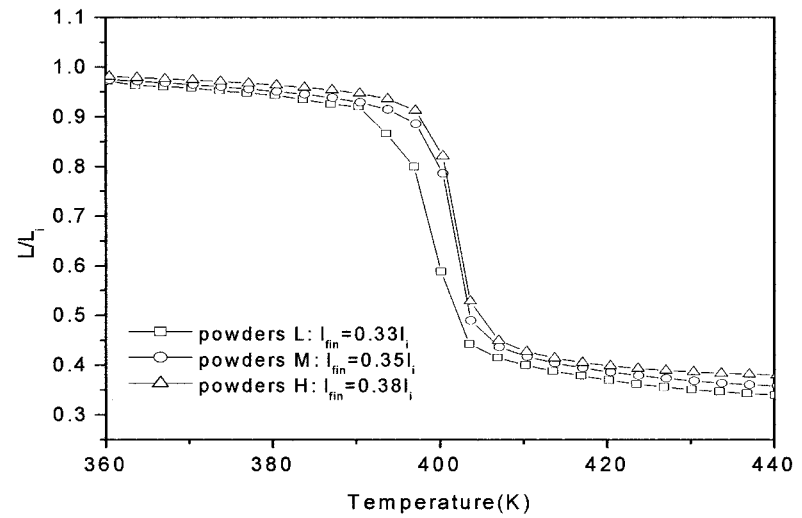

Figure 8 TMA sintering signal for powders L (□), M (○), and H (△).

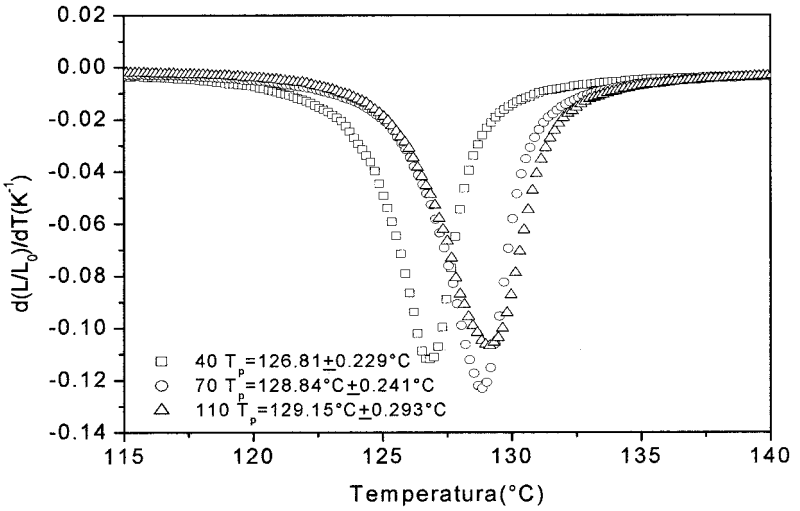

Figure 9 TMA rate of sintering for powders L (□), M (○), and H (△).

Further, the average bubble dimension is higher, a consequence of the higher dimension of the initial particles. The M powders show the lowest void content, which is also consistent with the particle size measurement, showing a minimum for M powders.

The sintering behavior was modeled using a kinetic model derived from the one proposed by Kandis and Bergman,[4] and modified to take into account the absence of sintering when the temperature is lower than the onset temperature of melting T_{on} (360 K as determined from DSC analysis). The equations used are

$$\frac{d\chi}{dt} = -k_0 \exp\left(-\frac{E}{R(T - T_{on})}\right)(\chi - \chi_\infty) \qquad (13)$$

$$\chi = 1 - \frac{\rho}{\rho_0} \qquad (14)$$

$$\rho = \rho_i \frac{L}{L_i}. \qquad (15)$$

where χ is the void fraction, χ_∞ is the final void fraction, E is the activation energy for sintering process, and K_0 is a preexponential factor. The final void fraction χ_∞ and initial density ρ_i can be determined using the data reported in Table IV, L/L_i is the output signal of TMA experiments, and the material density ρ_0 is taken as 950 kg/m^3. By nonlinear regression of TMA

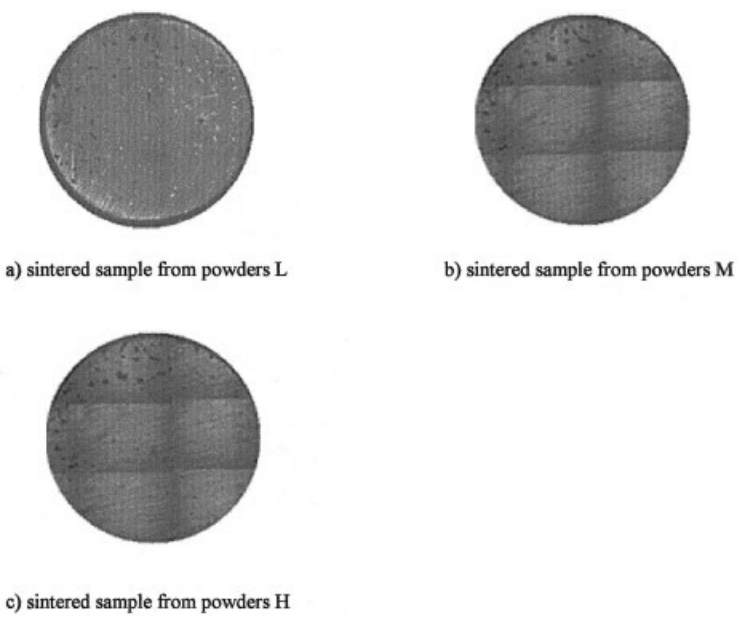

Figure 10 Sintered samples optical micrographs.

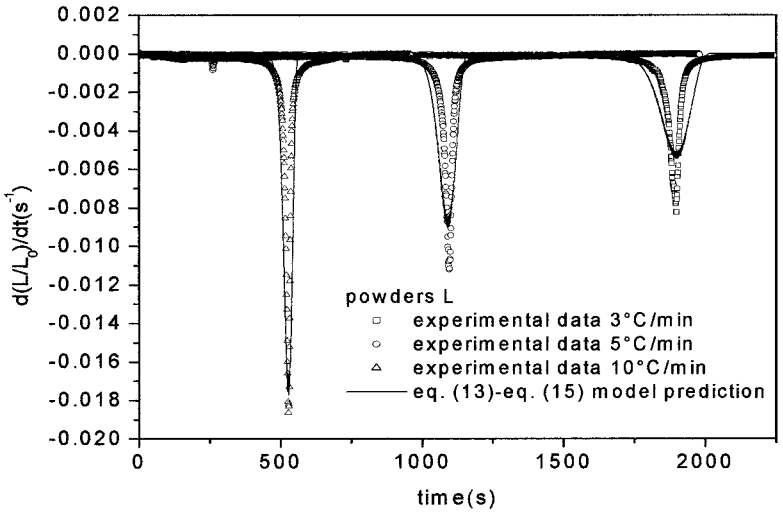

Figure 11 Sintering rate for powders L at 3 (□), 5 (○), and 10 (△) °C/min, and model prediction (—) according to eqs. (13)–(15).

experimental data values of the parameters E and K_0 were determined. The prediction according to the model of eqs. (13)–(15) is compared with experimental results in Figure 11 and Figure 12 for powders L and H, respectively. The values of E/R and k_0 calculated by nonlinear regression are reported in Table V.

The observed behavior of HDPE powders is in good agreement with experimental observations and theoretical modeling, predicting that the sintering rate strongly depends on initial particle size.[41] In particular, an increase of the milling temperature results in a higher activation energy for the sintering process, causing a shift of the whole process at slightly higher temperatures. This increase in activation energy is attributed to the more regular shape and larger size of H-type particles, discussed in detail previously.

CONCLUSIONS

In this work, the influence of grinding temperature on the shape and size of powders for rotational molding was studied. A quantitative approach to the description of the particles was presented. The efficiency of the shape factors for the powder characterization was well evidenced by the differences observed for powders obtained at different temperatures. The effect of the temperature on the shape of the particles indicated that larger and more regu-

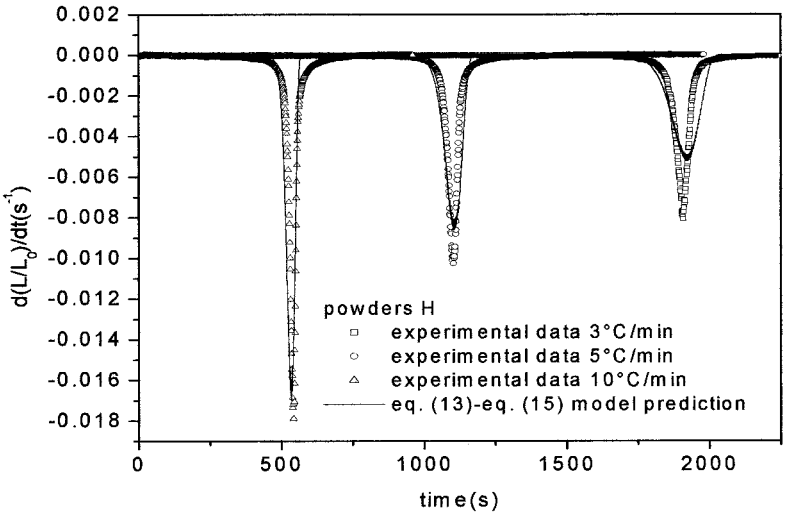

Figure 12 Sintering rate for powders H at 3 (□), 5 (○), and 10 (△) °C/min, and model prediction (—) according to eqs. (13)–(15).

TABLE V
Numerical Values for the Parameters of Eqs. (13)–(15) from Nonlinear Regression of Experimental Data

Parameter	Powders L	Powders H
k_0 (s^{-1})	4×10^6	4×10^6
E/R (K)	750	780

larly shaped particles are obtained by increasing the milling temperature.

The influence of particle size and shape was also reflected in the bulk properties of powders and in their sintering behavior. More regularly shaped particles had higher initial bulk density, although larger size was reflected in a less-efficient sintering process. The results obtained from the introduced mathematical model, and confirmed from experimental TMA observations, showed that an optimal milling temperature can be selected. When this temperature is approached, the apparent density of sintered products is higher, and good-quality rotational molded parts can be fabricated in processes, such as rotational molding, where the sintering behavior of powders plays a significant role in determining the final quality of the parts.

References

1. Beall, G. L. Plast Eng 1998, February, 33.
2. Bisaria, M. K.; Takacs, E.; Bellehumeur, C. T.; Vlachopoulos, J. Rotation 1994, Winter, 12.
3. Bellehumeur, C. T.; Bisaria, M. K.; Vlachopoulos, J. Polym Eng Sci 1996, 36, 2198.
4. Kandis, M.; Bergman, T. L. J Heat Transfer 1997, 119, 824.
5. Liu, S. J. Int Polym Proc 1998, 13, 88.
6. Kontopoulou, M.; Vlachopoulos, J. Polym Eng Sci 1999, 39, 1189.
7. Crawford, R. J. Rotational Molding of Plastics; Research Studies Press: Taunton, UK, 1992.
8. Rao, M. A.; Throne, J. L. Polym Eng Sci 1972, 12, 237.
9. Hsu, C. T.; Cheng, P.; Wong, K. W. Int J Heat Mass Transfer 1994, 37, 2751.
10. Zou, R. P.; Yu, A. B. Powder Technol 1996, 88, 71.
11. Tavman, I. H. Int Commun Heat Mass Transfer 1996, 23, 169.
12. Agapiou, J. S.; DeVries, M. F. J Heat Transfer 1989, 111, 281.
13. Bauer, T. H. Int J Heat Mass Transfer 1993, 36, 4181.
14. McDaid, J.; Crawford, R. J. Rotation 1997, Spring, 27.
15. Throne, J. L.; Sohn, M. S. Adv Polym Technol 1989, 9, 181.
16. Allen, M.; Brown, G. J.; Miles, N. J. Powder Technol 1995, 84, 1.
17. Kindratenko, V. V.; Treiger, B. A.; Van Espen, P. J. M. Chemom Intell Lab Syst 1996, 34, 103.
18. Panigrahi, S.; Misra, M. K.; Willson, S. Comput Electron Agric 1998, 20, 1.
19. Vertommen, J.; Rombaut, P.; Kinget, R. Int J Pharm 1997, 146, 21.
20. Wong, W. H.; Siu, W. C.; Lam, K. M. Pattern Recognit Lett 1995, 16, 115.
21. Baslev, I.; Doring, K.; Eriksen, R. D. Pattern Recognit Lett 2000, 21, 381.
22. Zhao, D.; Chen, J. Pattern Recognit 1997, 30, 895.
23. Zhu, Y.; De Silva, L. C.; Ko, C. C. Pattern Recognit Lett 2002, 23, 83.
24. Yang, L.; Albregtsen, F. Pattern Recognit 1996, 29, 1061.
25. Markopndeya Raj, P.; Cannon, W. R. Powder Technol 1999, 104, 180.
26. Lai, J. H.; Yuen, P. C.; Feng, G. C. Pattern Recognit 2001, 34, 95.
27. Hundal, H. S.; Rohani, S.; Wood, H. C.; Pons, M. N. Powder Technol 1997, 91, 217.
28. Drolon, H.; Druaux, F.; Faure, A. Pattern Recognit Lett 2000, 21, 473.
29. Newland, D. E. In: Proceedings of DETC 97, ASME Design Engineering Technical Conference, Sacramento, CA, 1997.
30. Greco, A.; Frigione, M.; Maffezzoli, A.; Acierno, D. Polym Recycl 2001, 6, 23.
31. Greco, A.; Maffezzoli, A. J Therm Anal Calorim, to appear.
32. Janowsky, J.; Sadowsky, A.; Kray, W.; Ratajczak, T. J Mater Sci 1998, 33, 477.
33. Stachowiak, G. W. Tribol Int 1998, 31, 139.
34. Dathe, A.; Eins, S.; Niemeyer, J.; Erold, G. Geoderma 2001, 103, 203.
35. Muniandy, S. V.; Moroz, I. M. Phys Lett A 1997, 253, 352.
36. Molina Boisseau, S.; Le Bolay, N.; Pons, M. Powder Technol 2002, 123, 282.
37. Shinohara, K.; Oida, M.; Golman, B. Powder Technol 2000, 107, 131.
38. Barnetson, A.; Hornsby, P. R. J Mater Sci Lett 1995, 14, 80.
39. Narkis, M.; Rosenberg, N. Polymer Powder Technology; Wiley: New York, 1995.
40. Nasar, R. S.; Cerqueira, M.; Longo, E.; Varala, J. A. Ceram Int 1999, 25, 593.
41. Kim, B. L.; Lee, J. H.; Kim, J. J.; Ikegami, T. Mater Lett 2002, 52, 114.